

Efficient and stable organic DSSC sensitizers bearing quinacridone and furan moieties as a planar π -spacer†

Jiabao Yang, Fuling Guo, Jianli Hua,* Xin Li, Wenjun Wu, Yi Qu and He Tian*

Received 28th March 2012, Accepted 24th May 2012

DOI: 10.1039/c2jm31929b

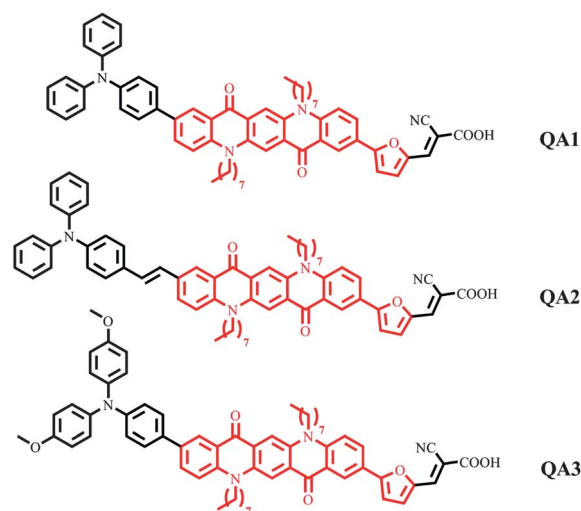
In this work, three new quinacridone-based dyes containing a furan moiety (**QA1–3**) have been synthesized through simple synthetic routes for the application of dye-sensitized solar cells (DSSCs). Their absorption spectra, electrochemical, photovoltaic properties and the cell long-term stability have been extensively investigated. Electrochemical measurement data indicates that the tuning of the HOMO and LUMO energy levels can be conveniently realized by alternating the donor moiety. The theoretical calculations show that the dihedral angle between the quinacridone moiety and the furan ring is less than 1 degree, indicating excellent planarity between the two groups, which is beneficial for intramolecular charge transfer. All of these dyes performed as sensitizers for DSSCs tested under similar AM 1.5 experimental conditions, and a maximum solar energy to electricity conversion efficiency of 7.70% ($J_{sc} = 13.25 \text{ mA cm}^{-2}$, $V_{oc} = 804 \text{ mV}$, $FF = 0.73$) for the 20 mM chenodeoxycholic acid (CDCA) co-adsorbed DSSCs based on **QA1** is obtained. Electrochemical impedance experiments indicate that the electron lifetime is improved by co-adsorption of CDCA, accounting for the significant improvement of V_{oc} . Most importantly, the long-term stability of the **QA1–3**-based DSSCs with ionic-liquid electrolytes under 1000 h light-soaking has been demonstrated.

Introduction

Solar energy, a renewable energy source, is generally considered as the most promising way to solve the global energy crisis. A variety of other light-harvesting devices were developed rapidly, including dye-sensitized solar cells (DSSCs),¹ which attracted great worldwide attention. As potential candidates for the future modality of photovoltaic cells, DSSCs manifest considerable efficiency and low cost, in which the sensitizer is deemed as the crucial component. At present, DSSC sensitizers based on Ru(II)-polypyridyl complexes have achieved power conversion efficiencies of nearly 12%.^{2,3} However, the large-scale application of Ru-complexes has become a critical problem due to limited resources and the hefty purification steps needed.⁴ Recently, a number of novel Ru-free sensitizers, such as phenoxazine,^{5,6} phenothiazine,^{7–9} diketo-pyrrolo-pyrrole^{10,11} and indoline,^{12–15} have been investigated and applied in DSSCs successfully. So far, impressive photovoltaic performances have been obtained using zinc porphyrin dye based DSSCs, which showed a power conversion efficiency exceeding 12%.¹⁶

Here we present three novel efficient dyes (**QA1–3**) (Scheme 1) with triarylamine as the donor, 5,12-dihydroquinone[2,3-*b*]

acridine-7,14-dione (quinacridone or QA) and furan units as the π -conjugated system and a cyanoacrylic acid moiety acting as acceptor. QA and its derivatives are well-known organic pigments with exceptional light, weather and heat stability,¹⁷ and they are not soluble in most common organic solvents due to the concurrent strong H-bonding and π - π intermolecular interactions in solid state. Soluble derivatives can be made by attaching long alkyl chains on the N atom positions of the QA moiety.^{18,19}

Scheme 1 Molecular structures of **QA1–QA3** dyes.

Key Laboratory for Advanced Materials and Institute of Fine Chemicals, East China University of Science & Technology, Shanghai 200237, P.R. China. E-mail: jlhua@ecust.edu.cn; tianhe@ecust.edu.cn; Fax: +86-21-64252758; Tel: +86-21-64250940

† Electronic supplementary information (ESI) available. See DOI: 10.1039/c2jm31929b

To some extent, the introduction of long alkyl chains into QA rings can also effectively inhibit the charge recombination and increase the electron lifetime.²⁰ At present, quinacridone-based molecular donors have been employed successfully in solution processed bulk-heterojunction organic solar cells and showed good performances.²¹ The triphenylamine can improve the hole transporting ability of the materials, and thanks to the nonplanar structure of triphenylamine, the formation of dye aggregates can also be relieved. Lately, triphenylamine-based dyes have been widely used in organic photovoltaic functional materials, especially in the field of solar cells.^{22–25} In addition, furan would be more efficient for hole location and reinforcing the stability of the dye-sensitizers owing to its smaller resonance energy (16 kcal mol⁻¹) in the spacer than the thiophene (29 kcal mol⁻¹) and benzene (36 kcal mol⁻¹).^{26,27} Hence, there have been some reports on incorporating a furan moiety into organic dyes as an alternative to thiophenes for photovoltaics, revealing that the optical and charge carrier mobility can be quite comparable to thiophenes.^{28–34} Most promisingly, furan derivatives can be obtained from a variety of natural products, and therefore dye-sensitizers containing a furan moiety can be considered as renewable and sustainable synthetic resources and the production of DSSCs on a large scale can be allowed.³⁵ To the best of our knowledge, there is only one report on the application of small molecular dyes containing quinacridone in DSSCs.³⁶ However, the quinacridone-based dyes only showed a PCE of 3.86%, for which the main reason may be the lack of efficient donors and too large a dihedral angle between the quinacridone moiety and thiophene or the benzene ring (19.8 and 33.6 degrees, respectively), resulting in less efficient intramolecular charge transfer (ICT).³⁶ Meanwhile, for QA-based sensitizers with different π -spacers (furan, thiophene, and benzene ring, Scheme S1†), we carried out density functional theory (DFT) at the B3LYP/6-31G* level in the gas phase. The theoretical calculations show that the dihedral angle between the quinacridone moiety and the furan ring is only 0.2 degrees, much smaller than that between the quinacridone moiety and thiophene or the benzene ring (16.4 and 32.3 degrees, respectively), indicating that the QA molecule bearing a furan moiety shows excellent planarity, which is beneficial for intramolecular charge transfer (ICT). Based on the consideration above, a new series of quinacridone-based dyes containing a furan moiety (QA1–3) were designed and synthesized (Scheme 1) as sensitizers for DSSCs. These dyes can be easily synthesized by a concise route and an environmentally-friendly procedure.

Experimental

Materials

Tetra-*n*-butylammonium hexafluorophosphate (TBAPF₆), 4-*tert*-butylpyridine (4-TBP), lithium iodide, and 2-cyanoacetic acid were purchased from Fluka. THF was pre-dried over 4 Å molecular sieves and distilled under an argon atmosphere from sodium benzophenone ketyl immediately prior to use. The starting materials 4-(*N,N*-diphenylamino) phenyl-boronic acid, *N,N*-diphenyl-4-vinylaniline and 4-(bis(4-methoxyphenyl)-amino)phenyl-boronic acid were synthesized according to the corresponding literature methods.^{8,37} All other solvents and chemicals were purchased from Aldrich and used as received

without further purification. Transparent FTO conducting glass (fluorine doped SnO₂, transmission >90% in the visible, sheet resistance 15 Ω per square) was obtained from Geao Science and Educational Co. Ltd. of China. Commercial TiO₂ (P25) was used for the preparation of the nanocrystalline films.

Spectroscopic measurements

¹H NMR spectra and ¹³C NMR spectra were obtained with a Brücker AM 400 spectrometer (relative to TMS). Mass spectra were recorded with a Waters LCT Premier XE spectrometer. Melting point measurements were performed with a SGW X-4 micro melting point meter. Elemental analysis was obtained with an Elementar Vario EL III spectrometer. The absorption spectra of the dyes in solution and adsorbed on TiO₂ films were measured with a Varian Cary 500 spectrophotometer.

Preparation of the solar cells

The dye-sensitized TiO₂ electrode was prepared by following the procedure reported in the literature.³⁸ A screen-printed double layer of TiO₂ particles was used as the photoelectrode. A 7 μ m thick film of 13 nm-sized TiO₂ particles (Ti-Nanoxide T/SP) was first printed on the FTO conducting glass and further coated with a 4 μ m thick second layer of 400 nm light-scattering anatase particles (Ti-Nanoxide 300). Sintering was carried out at 450 °C for 30 min. Before immersion in the dye solution, these films were soaked in 0.04 M aqueous TiCl₄ solution overnight in a closed chamber. After being washed with deionized water and fully rinsed with ethanol, the films were heated again at 450 °C for 30 min followed by cooling to 80 °C and dipping into a 3 \times 10⁻⁴ M solution of dyes in THF for 12 h at room temperature. For the co-adsorption, chenodeoxycholic acid was added with different concentrations. To prepare the counter electrode, Pt catalyst was deposited on cleaned FTO glass by coating with a drop of H₂PtCl₆ solution (0.02 M in 2-propanol solution) with heat treatment at 400 °C for 15 min. A hole (0.8 mm diameter) was drilled in the counter electrode by a drill-press. For the assembly of DSSCs, the dye-contained TiO₂ electrode and Pt-counter electrode were assembled into a sandwich-type cell and sealed with a hot-melt gasket of 25 μ m thickness made of the ionomer Surlyn 1702 (Dupont). The redox electrolyte was placed in a drilled hole in the counter electrode by capillary force, and was driven into the cell by means of vacuum backfilling. Two electrolytes were used for device evaluation, in which one was composed of 0.1 M lithium iodide, 0.6 M 1,2-dimethyl-3-propylimidazolium iodide (DMPII), 0.05 M I₂, and 0.5 M 4-*tert*-butylpyridine (4-TBP) in acetonitrile (AN) as the liquid electrolyte, and the other was composed of 0.1 M I₂, 0.1 M lithium iodide and 0.45 M benzimidazole (BI) in 1-propyl-3-methylimidazolium iodide (PMII) as the ionic liquid electrolyte. Finally, the hole was sealed using a UV-melt gum and a cover glass (0.1 mm thickness).

Photovoltaic performance measurements

Photovoltaic measurements employed an AM 1.5 solar simulator equipped with a 300 W xenon lamp (Model no. 91160, Oriel). The power of the simulated light was calibrated to 100 MW cm⁻² using a Newport Oriel PV reference cell system (Model 91150V).

I-*V* curves were obtained by applying an external bias to the cell and measuring the generated photocurrent with a Keithley model 2400 digital source meter. The voltage step and delay time of the photocurrent were 10 mV and 40 ms, respectively. The photocurrent action spectra were measured with an IPCE test system consisting of a Model SR830 DSP Lock-In Amplifier and a Model SR540 Optical Chopper (Stanford Research Corporation, USA), a 7IL/PX150 xenon lamp and power supply, and a 7ISW301 spectrometer.

Electrochemical measurements

The oxidation potentials of the dyes adsorbed on TiO₂ films were measured in a normal three-electrode electrochemical cell. A TiO₂ film stained with sensitizer was used as the working electrode, a platinum wire was the counter electrode, and a regular calomel electrode in saturated KCl solution was the reference electrode. The measurements were performed using a potentiostat/galvanostat model K0264 (Princeton Applied Research). The supporting electrolyte was 0.1 M TBAPF₆ (tetra-*n*-butylammonium hexafluorophosphate) with THF as the solvent. The electrochemical impedance spectroscopy (EIS) measurements of all the DSSCs were performed using a Zahner IM6e Impedance Analyzer (ZAHNER-Elektrik GmbH & CoKG, Kronach, Germany). The frequency range is 0.05 Hz–100 kHz. The applied voltage bias is –0.70 V. The magnitude of the alternating signal is 10 mV.

Synthesis

5,12-Dioctylquinolino[2,3-*b*]acridine-7,14-dione (1). 5,12-Dihydroquinolo[2,3-*b*]acridine-7,14-dione (4.68 g, 15 mmol) and tetrabutylammonium bromide (966 mg, 3 mmol) were dissolved in 100 mL toluene, and while stirring vigorously, 50% NaOH (20 mL) and *n*-octyl bromide (11.58 g, 60 mmol) were added slowly. The resulting mixture was heated to reflux for 24 h. The reaction was quenched with water (30 mL) and filtered. The organic layer from the filtrate was separated, and the solvent was removed under reduced pressure. The resulting crude product was purified by column chromatography, eluting with petroleum ether and methylene chloride (1 : 2, v/v) yielding the product as red solids (2.00 g, 24.9%). ¹H NMR (CDCl₃, 400 MHz), δ (TMS, ppm): 0.88–0.93 (m, 6H), 1.29–1.36 (m, 12H), 1.42–1.51 (m, 4H), 1.58–1.67 (m, 4H), 1.95–2.04 (m, 4H), 4.50 (t, *J* = 7.8 Hz, 4H), 7.22–7.30 (m, 2H), 7.51 (d, *J* = 8.8 Hz, 2H), 7.70–7.79 (m, 2H), 8.56 (dd, *J*₁ = 8.0 Hz, *J*₂ = 1.5 Hz, 2H), 8.76 (s, 2H).

2,9-Dibromo-5,12-dioctylquinolino[2,3-*b*]acridine-7,14-dione (2). 5,12-Dioctylquinolino[2,3-*b*]acridine-7,14-dione **1** (1.07 g, 2 mmol) and NBS (1.07 g, 6 mmol) in 50 mL CCl₄ were heated to reflux for 10 h. The mixture was cooled to room temperature and organic solution was removed by rotary evaporation. The residue was purified by column chromatography with silica gel using petroleum ether and methylene chloride (1 : 2, v/v) as eluent to yield 800 mg of a red powder (yield 57.6%). Melting point: 301 °C. ¹H NMR (CDCl₃, 400 MHz), δ (TMS, ppm): 0.87–0.94 (m, 6H), 1.30–1.39 (m, 12H), 1.41–1.50 (m, 4H), 1.53–1.65 (m, 4H), 1.83–1.97 (m, 4H), 4.34–4.42 (m, 4H), 7.27 (d, *J* = 9.2 Hz, 2H), 7.71 (dd, *J*₁ = 9.3 Hz, *J*₂ = 2.5 Hz, 2H), 8.45 (d, *J* = 2.5

Hz, 2H), 8.48 (s, 2H). ¹³C NMR (CDCl₃, 100 MHz), δ (TMS, ppm): 14.1, 22.7, 27.0, 29.3, 29.4, 31.8, 46.5, 113.9, 114.1, 116.9, 122.1, 126.0, 130.2, 135.5, 137.2, 140.9, 176.6. HRMS (ESI, *m/z*): [M + H]⁺ calcd for (C₃₆H₄₃N₃O₂Br₂): 693.1691; found: 693.1693.

2-Bromo-9-(4-(diphenylamino)phenyl)-5,12-dioctylquinolino[2,3-*b*]acridine-7,14-dione (3). Compound **2** (1.39 g, 2 mmol), 12.5 mL of 2.0 M K₂CO₃ aqueous solution and a catalytic amount of Pd(PPh₃)₄ (116 mg, 5 mol%) in 25 mL THF were heated to reflux for 0.5 h and then injected with 12.5 mL THF containing 4-(*N,N*-diphenylamino)phenyl-boronic acid (578 mg, 2 mmol). After refluxing for 12 h, the mixture was extracted with 100 mL of CH₂Cl₂. The organic portion was combined and removed by rotary evaporation. The residue was purified by column chromatography on silica using petroleum ether and methylene chloride (1 : 2, v/v) as eluent to yield 700 mg of a red powder (yield 40.7%). Melting point: 207 °C. ¹H NMR (CDCl₃, 400 MHz), δ (TMS, ppm): 0.87–0.93 (m, 6H), 1.28–1.42 (m, 12H), 1.42–1.52 (m, 4H), 1.57–1.66 (m, 4H), 1.90–2.01 (m, 4H), 4.42–4.51 (m, 4H), 7.03–7.09 (m, 2H), 7.15–7.20 (m, 6H), 7.25–7.32 (m, 5H), 7.48 (d, *J* = 9.1 Hz, 1H), 7.58 (d, *J* = 8.6 Hz, 2H), 7.68 (dd, *J*₁ = 9.2 Hz, *J*₂ = 2.5 Hz, 1H), 7.91 (dd, *J*₁ = 9.0 Hz, *J*₂ = 2.3 Hz, 1H), 8.54 (d, *J* = 2.5 Hz, 1H), 8.60 (s, 1H), 8.64 (s, 1H), 8.67 (d, *J* = 2.3 Hz, 1H). ¹³C NMR (CDCl₃, 100 MHz), δ (TMS, ppm): 14.8, 23.3, 27.8, 30.1, 32.5, 47.3, 47.4, 114.3, 114.5, 116.0, 117.3, 122.0, 123.8, 124.6, 125.3, 125.5, 126.8, 127.0, 128.1, 130.0, 131.0, 133.8, 133.9, 136.1, 137.9, 141.4, 141.7, 147.9, 148.3, 177.9. HRMS (ESI, *m/z*): [M + H]⁺ calcd for (C₅₄H₅₇N₃O₂Br): 858.3634; found: 858.3632.

(*E*)-2-Bromo-9-(4-(diphenylamino)styryl)-5,12-dioctylquinolino[2,3-*b*]acridine-7,14-dione (4). Compound **2** (1.39 g, 2 mmol), *N,N*-diphenyl-4-vinylaniline (542 mg, 2 mmol), Pd(OAc)₂ (6.5 mg, 0.03 mmol), tris(2-methylphenyl)phosphine (20 mg, 0.066 mmol) and triethylamine (0.5 mL) in 20 mL DMF under a nitrogen atmosphere were heated to react at 85 °C for 22 h. After cooling to room temperature, the mixture was poured into water and the precipitate was filtered. The residue was purified by column chromatography on silica using CH₂Cl₂/petroleum ether (2 : 1, v/v) to yield 180 mg of a red solid (yield: 10.2%). Melting point: 208 °C. ¹H NMR (CDCl₃, 400 MHz), δ (TMS, ppm): 0.87–0.93 (m, 6H), 1.28–1.41 (m, 12H), 1.41–1.51 (m, 4H), 1.57–1.66 (m, 4H), 1.89–1.99 (m, 4H), 4.39–4.48 (m, 4H), 7.02–7.11 (m, 6H), 7.12–7.16 (m, 4H), 7.25–7.31 (m, 5H), 7.36–7.44 (m, 3H), 7.70 (dd, *J*₁ = 9.2 Hz, *J*₂ = 2.5 Hz, 1H), 7.81 (dd, *J*₁ = 9.1 Hz, *J*₂ = 2.1 Hz, 1H), 8.40 (d, *J* = 2.0 Hz, 1H), 8.50 (d, *J* = 2.5 Hz, 1H), 8.54 (s, 1H), 8.58 (s, 1H). ¹³C NMR (CDCl₃, 100 MHz), δ (TMS, ppm): 14.1, 22.7, 25.9, 27.0, 29.3, 29.5, 31.8, 45.9, 115.1, 116.2, 123.0, 123.1, 123.2, 123.5, 124.6, 125.1, 125.7, 127.5, 128.0, 129.3, 130.3, 130.6, 131.2, 132.8, 135.1, 140.9, 141.1, 147.4, 147.5, 174.6. HRMS (ESI, *m/z*): [M + H]⁺ calcd for (C₅₆H₅₉N₃O₂Br): 884.3791; found: 884.3787.

2-(4-(Bis(4-methoxyphenyl)amino)phenyl)-9-bromo-5,12-dioctylquinolino[2,3-*b*]acridine-7,14-dione (5). The synthetic procedure for compound **5** was followed using **2** (695 mg, 1 mmol), 2.0 M K₂CO₃ aqueous solution (8 mL) and a catalytic amount of Pd(PPh₃)₄ (58 mg, 5 mol%) in 16 mL of THF which were heated to reflux for 0.5 h and then injected with 8 mL THF containing

4-(bis(4-methoxyphenyl)-amino)phenyl-boronic acid (349 mg, 1 mmol). The pure product was separated by a silica gel column chromatography using CH_2Cl_2 /petroleum ether (2 : 1, v/v) to yield 320 mg of a red solid (yield 34.8%). Melting point: 204 °C. ^1H NMR (CDCl_3 , 400 MHz), δ (TMS, ppm): 0.87–0.92 (m, 6H), 1.28–1.40 (m, 12H), 1.44–1.50 (m, 4H), 1.58–1.65 (m, 4H), 1.89–2.00 (m, 4H), 3.82 (s, 6H), 4.40–4.49 (m, 4H), 6.85–6.89 (m, 4H), 7.03 (d, $J = 8.7$ Hz, 2H), 7.11–7.14 (m, 4H), 7.28 (d, $J = 9.3$ Hz, 1H), 7.44 (d, $J = 9.2$ Hz, 1H), 7.52 (d, $J = 8.7$ Hz, 2H), 7.66 (dd, $J_1 = 9.2$ Hz, $J_2 = 2.5$ Hz, 1H), 7.89 (dd, $J_1 = 9.0$ Hz, $J_2 = 2.3$ Hz, 1H), 8.53 (d, $J = 2.5$ Hz, 1H), 8.57 (s, 1H), 8.63 (s, 1H), 8.64 (d, $J = 2.4$ Hz, 1H). ^{13}C NMR (CDCl_3 , 100 MHz), δ (TMS, ppm): 14.1, 22.7, 27.0, 27.2, 29.3, 29.4, 29.6, 31.8, 55.5, 113.6, 114.8, 116.9, 120.6, 121.2, 124.3, 126.7, 127.2, 131.1, 133.0, 133.5, 133.8, 135.1, 135.5, 137.3, 140.8, 148.0, 156.0, 170.2. HRMS (ESI, m/z): $[\text{M} + \text{H}]^+$ calcd for ($\text{C}_{56}\text{H}_{61}\text{N}_3\text{O}_4\text{Br}$): 918.3845; found: 918.3850.

5-(9-(4-(Diphenylamino)phenyl)-5,12-dioctyl-7,14-dioxo-5,7,12,14-tetrahydroquinolino[2,3-*b*]acridin-2-yl)furan-2-carbaldehyde (6). Compound **3** (257 mg, 0.3 mmol), 2.0 M K_2CO_3 aqueous solution (12.5 mL) and a catalytic amount of $\text{Pd}(\text{PPh}_3)_4$ (17 mg, 5 mol %) in 25 mL THF were heated to reflux for 0.5 h and then injected with 12.5 mL THF containing 5-formyl-2-furanylboronic acid (84 mg, 0.6 mmol), and the mixture was reacted at reflux for 12 h. After cooling to room temperature, the mixture was extracted with 100 mL of CH_2Cl_2 . The organic portion was combined and removed by rotary evaporation. The residue was purified by column chromatography on silica (methylene chloride as eluent) to yield 250 mg of a red solid (yield 95.4%). Melting point: 213 °C. ^1H NMR (CDCl_3 , 400 MHz), δ (TMS, ppm): 0.90 (t, $J = 6.7$ Hz, 6H), 1.30–1.44 (m, 12H), 1.45–1.55 (m, 4H), 1.57–1.70 (m, 4H), 1.95–2.06 (m, 4H), 4.48–4.56 (m, 4H), 6.88 (d, $J = 3.7$ Hz, 1H), 7.06 (t, $J = 7.3$ Hz, 2H), 7.14–7.19 (m, 6H), 7.27–7.32 (m, 4H), 7.34 (d, $J = 3.7$ Hz, 1H), 7.50 (t, $J = 7.9$ Hz, 2H), 7.54–7.57 (m, 2H), 7.88 (dd, $J_1 = 9.1$ Hz, $J_2 = 2.3$ Hz, 1H), 8.08 (dd, $J_1 = 9.0$ Hz, $J_2 = 2.0$ Hz, 1H), 8.62 (s, 1H), 8.67 (d, $J = 2.2$ Hz, 1H), 8.68 (s, 1H), 8.77 (d, $J = 2.1$ Hz, 1H), 9.64 (s, 1H). ^{13}C NMR (CDCl_3 , 100 MHz), δ (TMS, ppm): 14.1, 22.7, 27.1, 29.4, 31.8, 46.9, 107.6, 113.5, 115.2, 115.4, 118.2, 118.3, 121.2, 123.0, 123.8, 124.5, 124.6, 124.7, 126.0, 126.2, 127.3, 129.4, 130.8, 132.9, 135.0, 135.6, 142.3, 147.6, 151.9, 158.5, 177.3, 177.9. HRMS (ESI, m/z): $[\text{M} + \text{H}]^+$ calcd for ($\text{C}_{59}\text{H}_{60}\text{N}_3\text{O}_4$): 874.4584; found: 874.4579.

(E)-5-(9-(4-(Diphenylamino)styryl)-5,12-dioctyl-7,14-dioxo-5,7,12,14-tetrahydroquinolino[2,3-*b*]acridin-2-yl)furan-2-carbaldehyde (7). The synthesis method resembles that of compound **6** and the compound was purified by column chromatography on silica (CH_2Cl_2 as eluent) to yield 120 mg of a dark red solid (yield 86.9%). Melting point: 216 °C. ^1H NMR (CDCl_3 , 400 MHz), δ (TMS, ppm): 0.89–0.95 (m, 6H), 1.30–1.45 (m, 12H), 1.45–1.55 (m, 4H), 1.61–1.70 (m, 4H), 1.91–2.04 (m, 4H), 4.40–4.50 (m, 4H), 6.79–6.81 (m, 1H), 6.94 (d, $J = 7.2$ Hz, 2H), 7.02–7.08 (m, 4H), 7.14 (d, $J = 7.5$ Hz, 4H), 7.25–7.32 (m, 5H), 7.32–7.38 (m, 3H), 7.41–7.45 (m, 1H), 7.70 (dd, $J_1 = 9.1$ Hz, $J_2 = 2.0$ Hz, 1H), 7.96 (dd, $J_1 = 9.0$ Hz, $J_2 = 2.1$ Hz, 1H), 8.25 (d, $J = 2.0$ Hz, 1H), 8.42 (s, 1H), 8.49 (s, 1H), 8.56 (d, $J = 2.2$ Hz, 1H), 9.59 (s, 1H). ^{13}C NMR (CDCl_3 , 100 MHz), δ (TMS, ppm): 14.0, 22.5,

26.1, 27.2, 29.2, 30.6, 45.9, 106.6, 112.5, 113.2, 114.0, 114.2, 117.8, 118.5, 121.8, 124.0, 124.2, 124.5, 125.8, 126.2, 126.5, 126.8, 127.3, 130.4, 131.4, 133.1, 136.0, 138.1, 141.2, 145.6, 150.9, 156.5, 174.3, 175.2. HRMS (ESI, m/z): $[\text{M} + \text{H}]^+$ calcd for ($\text{C}_{61}\text{H}_{62}\text{N}_3\text{O}_4$): 900.4740; found: 900.4737.

5-(9-(4-(Bis(4-methoxyphenyl)amino)phenyl)-5,12-dioctyl-7,14-dioxo-5,7,12,14-tetrahydroquinolino[2,3-*b*]acridin-2-yl)furan-2-carbaldehyde (8). The synthesis method resembles that of compound **6** and the compound was purified by column chromatography on silica (CH_2Cl_2 as eluent) to yield 148 mg of a dark red solid (yield 86.8%). Melting point: 212 °C. ^1H NMR (CDCl_3 , 400 MHz), δ (TMS, ppm): 0.87–0.94 (m, 6H), 1.30–1.43 (m, 12H), 1.43–1.53 (m, 4H), 1.60–1.69 (m, 4H), 1.95–2.05 (m, 4H), 3.82 (s, 6H), 4.47–4.56 (m, 4H), 6.84–6.91 (m, 5H), 6.99–7.05 (m, 2H), 7.06–7.15 (m, 4H), 7.33–7.37 (m, 1H), 7.48–7.55 (m, 4H), 7.89 (d, $J = 8.0$ Hz, 1H), 8.11 (d, $J = 8.8$ Hz, 1H), 8.64 (s, 1H), 8.67 (s, 1H), 8.71 (s, 1H), 8.80 (s, 1H), 9.64 (s, 1H). ^{13}C NMR (CDCl_3 , 100 MHz), δ (TMS, ppm): 14.0, 22.7, 26.1, 30.4, 31.6, 32.4, 46.6, 48.8, 105.1, 110.5, 112.9, 113.4, 116.8, 117.5, 117.7, 120.2, 123.4, 123.9, 125.5, 125.7, 125.9, 126.2, 126.9, 129.0, 129.3, 131.8, 132.0, 133.2, 134.6, 140.4, 144.2, 146.9, 148.5, 156.9, 175.3, 175.7. HRMS (ESI, m/z): $[\text{M} + \text{H}]^+$ calcd for ($\text{C}_{61}\text{H}_{64}\text{N}_3\text{O}_6$): 934.4795; found: 934.4789.

2-Cyano-3-(5-(9-(4-(diphenylamino)phenyl)-5,12-dioctyl-7,14-dioxo-5,7,12,14-tetrahydroquinolino[2,3-*b*]acridin-2-yl)furan-2-yl)acrylic acid (QA1). Compound **6** (140 mg, 0.16 mmol), 2-cyanoacetic acid (85 mg, 1 mmol) and ammonium acetate (3 mg, 0.039 mmol) in 20 mL acetic acid were heated to reflux under a nitrogen atmosphere for 12 h. After cooling to room temperature, the precipitate was filtered and recrystallized with THF/EtOH to yield 130 mg of a red solid (yield 86.3%). Melting point: 306 °C. ^1H NMR (THF- d_8 , 400 MHz), δ (TMS, ppm): 0.80–0.85 (m, 6H), 1.24–1.38 (m, 12H), 1.40–1.50 (m, 4H), 1.51–1.61 (m, 4H), 1.85–1.95 (m, 4H), 4.40–4.50 (m, 4H), 6.88–6.94 (m, 2H), 6.99–7.05 (m, 7H), 7.13–7.18 (m, 4H), 7.24–7.27 (m, 1H), 7.42–7.46 (m, 2H), 7.50 (d, $J = 9.2$ Hz, 1H), 7.60 (d, $J = 9.2$ Hz, 1H), 7.72 (dd, $J_1 = 9.0$ Hz, $J_2 = 2.1$ Hz, 1H), 7.76 (s, 1H), 8.01 (dd, $J_1 = 9.0$ Hz, $J_2 = 1.9$ Hz, 1H), 8.36 (s, 1H), 8.40–8.43 (m, 1H), 8.45–8.48 (m, 2H). ^{13}C NMR (THF- d_8 , 100 MHz), δ (TMS, ppm): 13.5, 22.6, 26.8, 29.4, 31.8, 46.1, 54.0, 61.4, 77.3, 86.8, 91.6, 93.0, 93.9, 103.0, 104.8, 108.7, 113.5, 114.2, 114.6, 120.8, 122.8, 123.9, 124.2, 124.4, 124.7, 125.8, 127.2, 128.3, 132.3, 133.7, 138.5, 142.0, 142.5, 146.1, 147.2, 147.8, 149.6, 158.8, 163.3, 181.2, 182.6, 183.2. HRMS (ESI, m/z): $[\text{M} + \text{H}]^+$ calcd for ($\text{C}_{62}\text{H}_{61}\text{N}_4\text{O}_5$): 941.4642; found: 941.4644. Anal. calcd for ($\text{C}_{62}\text{H}_{60}\text{N}_4\text{O}_5$): C 79.12, H 6.43, N 5.95; found: C 79.01, H 6.34, N 5.88%.

2-Cyano-3-(5-(9-(4-(diphenylamino)styryl)-5,12-dioctyl-7,14-dioxo-5,7,12,14-tetrahydroquinolino[2,3-*b*]acridin-2-yl)furan-2-yl)acrylic acid (QA2). The synthesis method resembles that of compound **QA1** and the compound was recrystallized with THF/EtOH to yield 99 mg of a dark red solid (yield: 83.8%). Melting point: 310 °C. ^1H NMR (THF- d_8 , 400 MHz), δ (TMS, ppm): 0.80–0.86 (m, 6H), 1.23–1.37 (m, 12H), 1.39–1.50 (m, 4H), 1.51–1.59 (m, 4H), 1.86–1.98 (m, 4H), 4.43–4.52 (m, 4H), 6.88–6.94 (m, 4H), 6.96–7.04 (m, 6H), 7.06–7.09 (m, 1H), 7.12–7.17 (m, 4H), 7.28–7.31 (m, 1H), 7.34–7.39 (m, 2H), 7.49 (d, $J = 9.0$ Hz,

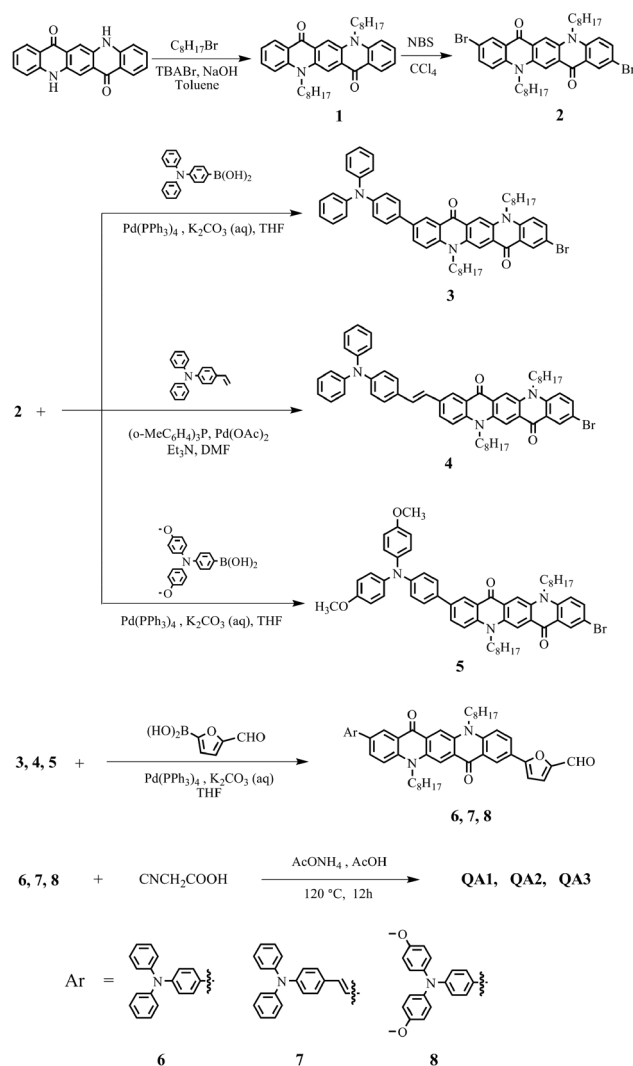
1H), 7.66 (d, $J = 9.1$ Hz, 1H), 7.78 (d, $J = 9.1$ Hz, 1H), 7.83 (s, 1H), 8.12 (d, $J = 9.0$ Hz, 1H), 8.27 (s, 1H), 8.46 (s, 1H), 8.53 (s, 1H), 8.59 (s, 1H). ^{13}C NMR (THF- d_8 , 100 MHz), δ (TMS, ppm): 11.6, 20.7, 27.6, 30.0, 54.1, 76.1, 76.4, 76.7, 79.9, 81.7, 82.1, 88.4, 100.5, 101.0, 103.5, 104.5, 105.8, 106.7, 110.5, 111.4, 112.2, 113.2, 117.8, 119.9, 121.7, 122.5, 125.4, 126.8, 127.2, 127.5, 128.2, 128.7, 129.5, 130.2, 132.1, 135.8, 140.5, 145.9, 147.8, 150.9, 153.2, 156.9, 161.4, 161.9, 182.8, 186.7, 187.6. HRMS (ESI, m/z): $[M + H]^+$ calcd for ($\text{C}_{64}\text{H}_{63}\text{N}_4\text{O}_5$): 967.4798; found: 967.4805. Anal. calcd for ($\text{C}_{64}\text{H}_{62}\text{N}_4\text{O}_5$): C 79.48, H 6.46, N 5.79; found: C 79.30, H 6.32, N 5.61%.

3-(5-(9-(4-(Bis(4-methoxyphenyl)amino)phenyl)-5,12-dioctyl-7,14-dioxo-5,7,12,14-tetrahydroquinolino[2,3-*b*]acridin-2-yl) furan-2-yl)-2-cyanoacrylic acid (QA3). The synthesis method resembles that of compound QA1 and the compound was recrystallized with THF/EtOH to yield 115 mg of a dark red solid (yield: 80.7%). Melting point: 299 °C. ^1H NMR (THF- d_8 , 400 MHz), δ (TMS, ppm): 0.89–0.94 (m, 6H), 1.34–1.48 (m, 12H), 1.49–1.59 (m, 4H), 1.75–1.82 (m, 4H), 1.97–2.06 (m, 4H), 3.77 (s, 6H), 4.56–4.65 (m, 4H), 6.86 (d, $J = 8.8$ Hz, 4H), 6.98 (d, $J = 8.6$ Hz, 2H), 7.07 (d, $J = 8.8$ Hz, 4H), 7.20 (d, $J = 3.7$ Hz, 1H), 7.41 (d, $J = 3.8$ Hz, 1H), 7.51 (d, $J = 8.6$ Hz, 2H), 7.67 (d, $J = 9.1$ Hz, 1H), 7.81 (d, $J = 9.3$ Hz, 1H), 7.92 (d, $J = 8.8$ Hz, 1H), 7.94 (s, 1H), 8.27 (d, $J = 8.7$ Hz, 1H), 8.59 (d, $J = 2.1$ Hz, 1H), 8.63 (s, 1H), 8.71 (s, 1H), 8.77 (d, $J = 2.0$ Hz, 1H). ^{13}C NMR (THF- d_8 , 100 MHz), δ (TMS, ppm): 13.5, 22.6, 29.5, 29.4, 31.9, 54.8, 68.9, 72.4, 74.3, 78.7, 97.8, 100.1, 111.8, 114.4, 115.6, 120.6, 121.5, 126.5, 126.9, 130.5, 131.6, 135.7, 137.1, 137.3, 138.5, 138.7, 143.3, 151.1, 151.3, 156.3, 157.4, 158.8, 163.9, 172.6, 174.7, 178.8. HRMS (ESI, m/z): $[M + H]^+$ calcd for ($\text{C}_{64}\text{H}_{65}\text{N}_4\text{O}_7$): 1001.4853; found: 1001.4856. Anal. calcd for ($\text{C}_{64}\text{H}_{64}\text{N}_4\text{O}_7$): C 76.78, H 6.44, N 5.60; found: C 76.58, H 6.36, N 5.46%.

Results and discussion

Synthesis

The synthetic route to the three dyes QA1–3 containing quinacridone moiety is depicted in Scheme 2. The octyl attached to the quinacridone group can improve the solubility, forming a tightly packed insulating monolayer blocking the I_3^- or cations from approaching the TiO_2 and enhancing the open circuit voltage. The synthesis of QA1–3 was started from a commercially available quinacridone precursor. The *N*-alkylation of quinacridone gave **1**, in which the bromination of **1** with *N*-bromosuccinimide (NBS) provided compound **2** in good yield. Asymmetrical Suzuki coupling reaction of compound **2** with 4-(diphenylamino)phenyl-boronic acid and 4-(bis(4-methoxyphenyl)-amino)phenyl-boronic acid gave compounds **3** and **5**, respectively. Heck reaction of **2** with *N,N*-diphenyl-4-vinylaniline provided compound **4**. In the next step, Suzuki coupling of **3–5** with 5-formyl-2-furanylboronic acid afforded monoaldehyde substituted precursors **6–8**, respectively. Finally, the target products (QA1–3) were obtained *via* Knoevenagel condensation reaction of the respective aldehydes with 2-cyanoacetic acid in the presence of ammonium acetate. All the intermediates and target dyes were confirmed by standard spectroscopic methods.



Scheme 2 The synthetic procedure of the dyes QA1–3.

Spectroscopic properties of QA1–3 in solution and adsorbed on TiO_2 films

The UV-Vis absorption spectra of the three dyes QA1–3 in THF solutions and on TiO_2 films are shown in Fig. 1, and their absorption data are listed in Table 1. In the UV-Vis spectra in Fig. 1a, these dyes exhibit three major prominent bands, appearing at 300–390 nm, 400–500 nm, and 520–570 nm, respectively. The former shows typical triarylamine absorption

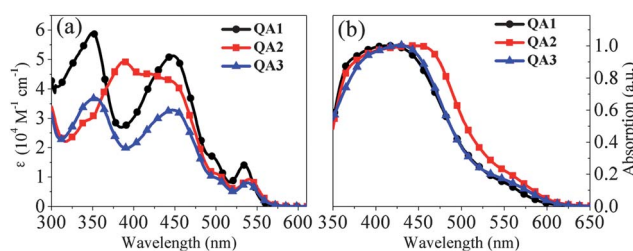


Fig. 1 UV-Vis absorption spectra of QA1–3 in THF solutions (a) and on TiO_2 films (7 μm) (b).

Table 1 Photophysical and electrochemical properties of dyes

Dye	$\lambda_{\max}^a/\text{nm}^{-1}$ ($\epsilon \times 10^{-4}$ M cm)	$\lambda_{\max}^b/\text{nm}^{-1}$	HOMO ^c /V ⁻¹ (vs. NHE)	E_{0-0}^d/V^{-1}	LUMO ^e /V ⁻¹ (vs. NHE)
QA1	534 (1.38), 446 (5.12), 350 (5.88)	416	1.06	2.03	-0.97
QA2	540 (0.93), 447 (4.34), 388 (4.92)	447	0.99	1.99	-1.00
QA3	539 (0.80), 447 (3.28), 352 (3.69)	432	0.83	2.01	-1.18

^a Absorption maximum in THF solution at room temperature. ^b Absorption maximum on TiO₂ film (without CDCA). ^c HOMOs were measured in THF with 0.1 M tetrabutylammonium hexafluorophosphate (TBAPF₆) as electrolyte (working electrode: FTO/TiO₂/dye; reference electrode: SCE; calibrated with ferrocene/ferrocenium (Fc/Fc⁺) as an external reference and converted to NHE by addition of 0.07 V. Counter electrode: Pt). ^d E_{0-0} was estimated from the absorption thresholds from the absorption spectra of dyes adsorbed on the TiO₂ film. ^e LUMO is estimated by subtracting E_{0-0} from HOMO.

peaks at 350/388/352 nm in THF,¹⁹ respectively, in which the peak of **QA2** at 388 nm shows about a 40 nm red-shift because of the conjugation between triphenylamine and vinyl. The middle band of **QA1–3** is ascribed to a localized aromatic $\pi-\pi^*$ transition of quinacridone with furan and the terminal cyanoacrylic acid group, in which **QA1–3** show an absorption peak at around 446 nm in THF. It is demonstrated by the measurement of the UV-Vis absorption of the intermediates 1,3,5-(9-bromo-5,12-dioctyl-7,14-dioxo-5,7,12,14-tetrahydroquinolino[2,3-*b*]acridin-2-yl)furan-2-carbaldehyde (**a**), 3-(5-(9-bromodicyoctyl-7,14-dioxo-5,7,12,14-tetrahydroquinolino-[2,3,5,12-*b*]acridin-2-yl)furan-2-yl)-2-cyanoacrylic acid (**b**) and **QA1** in THF solutions (Fig. S1†). Meanwhile, time-dependent density functional theory (TDDFT) calculations were carried out with the solvent effects of THF taken into account by the polarizable continuum model (PCM). The PBE0 functional was used together with the 6-31G* basis set (Table S1 and S2†). The largest oscillator strengths (*f*) around 450 nm correspond to excitation from HOMO–1 to LUMO. The molecular orbital image shows that the transition is consistent with our experimental attribution.

The bands at around 520–570 nm can be attributed to the intramolecular charge transfer (ICT) between the triarylamine donor and the acceptor. For the charge-transfer band, the absorption maxima for **QA1–3** in THF are at 534 nm, 540 nm and 539 nm, respectively. Compared with **QA1** and **QA3**, **QA2** has a vinyl group between triphenylamine and the QA moiety, which enhanced the extent of electron delocalization over the whole molecule, so its maximum absorption peak was red shifted. At the same time the absorption band of **QA3** shows a slight red-shift compared with **QA1** due to the effect of the two methoxy groups attached to the triphenylamine on the electron donor side. It is worth noting that the corresponding maximum extinction coefficients of the three dyes at around 446 nm are higher than that of the band at around 540 nm, in which they are 5.12×10^4 , 4.34×10^4 and 3.28×10^4 M⁻¹ cm⁻¹, respectively. In comparison with conventional ruthenium complexes (for example, 1.39×10^4 M⁻¹ cm⁻¹ at 541 nm for N₃),³⁹ the present dye molecules show about three times higher absorption coefficients. A corresponding thinner nanocrystalline film is allowed owing to the greater maximum absorption coefficients of the organic dyes, which could be beneficial for DSSCs with an ionic liquid electrolyte for better conversion efficiencies.⁴

Fig. 1b shows the absorption spectra of **QA1–3** on 7 μm transparent TiO₂ films after 10 h adsorption. Compared to the spectrum in THF solution, the absorption peaks for **QA1–3** on TiO₂ films are blue-shifted by 30, 3 and 15 nm, respectively.

Generally, due to the strong attractive force between the molecules, they have a strong tendency to aggregate in solution or at the solid–liquid interface when the sensitizers are adsorbed onto a nanocrystalline TiO₂ surface. Dye aggregates usually have three forms: red-shifted J-aggregates, blue-shifted H-aggregates and both red- and blue-shifted herring-bone aggregates.⁴⁰ The experimental results indicate that **QA1–3** used in this work form H-aggregates on the TiO₂ nanocrystal surface. On the other hand, after the sensitizer molecule adsorbs on TiO₂ film, the decreased electron-withdrawing ability of the acceptor (cyanoacrylic acid group) can also cause the blue-shifted absorption spectra. Therefore, the blue-shifted absorption spectra of the dyes on TiO₂ are attributed to the H-aggregates and deprotonation of the carboxylic acid. In addition, it is noteworthy that the absorption spectra of those dyes anchored onto transparent TiO₂ show an obviously broad profile, which is beneficial for light-harvesting.

Electrochemical properties of QA1–3

To evaluate the possibility of electron transfer from the excited dye to the conduction band (CB) of TiO₂, the highest occupied molecular orbital (HOMO) and lowest unoccupied molecular orbital (LUMO) energy levels are usually employed by means of cyclic voltammetry (CV) measurements of these dyes. The CV measurements of **QA1–3** were performed in tetrahydrofuran solution, using 0.1 M tetrabutylammonium hexafluorophosphate as the supporting electrolyte, Pt as the counter electrode and a saturated calomel electrode (SCE) as the reference electrode. Two sets of measurement were carried out for comparison, one employing TiO₂ films stained with sensitizers as the working electrode and the other with the sensitizer dissolved in THF solution. The SCE reference electrode was calibrated using a ferrocene/ferrocenium (Fc/Fc⁺) redox couple as an external standard and the $E_{1/2}$ of the Fc/Fc⁺ redox couple was found to be 0.56 V *versus* the SCE reference electrode. The potentials *versus* NHE were calibrated by the addition of 0.63 V to the potentials *versus* Fc/Fc⁺.⁷ Therefore, the potentials measured *vs.* SCE were converted to normal hydrogen electrode (NHE) by the addition of 0.07 V. The voltammetric results are presented in Fig. S2†, and the data on the films are collected in Table 1. The first half-wave potentials of **QA1–3** on the films are 0.99 V, 0.92 V and 0.76 V (*vs.* SCE). Therefore, the HOMO levels of **QA1–3** corresponding to their first redox potential are 1.06 V, 0.99 V and 0.83 V *vs.* NHE, respectively, which are much more positive than the iodine/iodide redox potential value (0.4 V *vs.*

NHE), ensuring that there is enough driving force for the efficient dye regeneration through the recapture of the injected electrons from I^- by the dye cationic radical. The excitation transition energy (E_{0-0}) of **QA1–3** is estimated from their absorption thresholds of dye-sensitized TiO_2 films to be 2.03 V, 1.99 V and 2.01 V, respectively. The estimated excited state potentials corresponding to the LUMO levels of **QA1–3**, calculated from $E_{HOMO} - E_{0-0}$, are -0.97 V, -1.00 V and -1.18 V vs. NHE, respectively. Thanks to the more negative LUMO values of the three dyes compared to the bottom of the conduction band of TiO_2 (-0.5 V vs. NHE), the electron injection process from the excited dye molecule to the TiO_2 conduction band is energetically permitted.

To scrutinize the electronic properties of these dyes further, the optimized structures and electron distribution of the HOMOs and LUMOs of **QA1–3** performed by density functional theory (DFT) at the B3LYP/6-31G* level in the gas phase are shown in Table S3 and S4†, respectively. The theoretical calculations show that the dihedral angle between the quinacridone ring and the furan ring is less than 1 degree, which is beneficial for intramolecular charge transfer. As shown in Table S4†, the HOMOs in **QA1–3** are primarily located on the π -framework of the donor part (triphenylamine), while the electron density of the LUMOs is delocalized over the furan group and anchoring group. Thus, the electron distribution from the donor unit to the anchoring moiety can be moved by excitation from the HOMO to the LUMO orbital to realize electron injection into the conduction band of TiO_2 .

Photovoltaic performances of DSSCs based on QA1–3

The DSSCs were prepared by using a dye-absorbed TiO_2 electrode, Pt-coated glass as the counter electrode, and an acetonitrile solution with iodine (0.05 M), lithium iodide (0.1 M), 1,2-dimethyl-3-propylimidazolium iodide (0.6 M), and 4-*tert*-butylpyridine (0.5 M) as the electrolyte. Fig. 2a shows the incident photon-to-electron conversion efficiency (IPCE) as a function of incident wavelength for DSSCs based on these dyes. The solar cells based on **QA1–3** show high IPCEs above 60% in the range of 450–605 nm and with the highest values of 83% at 570 nm for **QA1**, 77% at 550 nm for **QA2** and 75% at 535 nm for **QA3**, respectively. Meanwhile the IPCE values for **QA1–3** are obviously decreased at 610 to 680 nm, which is in accordance with their absorption spectra on the TiO_2 film. However, compared to the absorption spectra of sensitized films, the IPCE spectra are broadened significantly. The scattering effect of the

large particles in the film and the reflective effect of the Pt counter electrode can be considered as reasonable interpretations.¹³ The IPCE of **QA1** is higher than those of **QA2** and **QA3** in the region from 400 nm to 605 nm, though the IPCE values of **QA1** compared to **QA2** and **QA3** are slightly lower in the region of 610–680 nm, indicating that the **QA1** sensitized TiO_2 electrode would generate a higher conversion yield among the three dyes.

Fig. 2b shows the current–voltage characteristics of the DSSCs fabricated with **QA1–3** as sensitizers under standard global AM 1.5 solar light conditions. The detailed parameters of short-circuit current density (J_{sc}), open-circuit voltage (V_{oc}), fill factor (FF), and photovoltaic conversion efficiency (η) are summarized in Table 2. Generally, J_{sc} is related to the molar extinction coefficient of the dye molecule, in which a higher molar extinction coefficient has good light-harvesting ability and yields a higher short circuit, correspondingly. **QA1** dye has the highest light harvesting efficiency and consequently an improved J_{sc} due to the largest molar extinction coefficient. It is noteworthy that all of the three dyes have higher open circuit voltages (V_{oc}) (773–794 mV) than **N719** (726 mV) measured under the same conditions. The reason is that the introduction of two hydrophobic alkyl chains into the quinacridone rings can act as barriers preventing hydrophilic I_3^- from approaching the TiO_2 surface, inhibiting charge recombination and thus improving V_{oc} . **QA2**-based DSSCs show a lower V_{oc} (773 mV) than **QA1** and **QA3**-based DSSCs. One plausible explanation is that the extended conjugation and good planarity can enhance the charge recombination and result in a lower V_{oc} .^{41,42} The dark current–voltage characteristics also agree well with the V_{oc} values, in which the quinacridone-bridged dyes' dark current onset potential shifted to a larger value than **N719**. DSSCs based on **QA1** exhibit the best overall light to electricity conversion efficiency of 6.80% ($J_{sc} = 12.42$ mA cm⁻², $V_{oc} = 776$ mV, FF = 0.71) under AM 1.5 irradiation (100 mW cm⁻²), which reached 87% with respect to that of an **N719**-based device fabricated under similar conditions.

Due to strong intermolecular interactions, π – π stacking of organic dye molecules usually occurs, causing inefficient electron injection and low power conversion efficiency.⁴³ It has been demonstrated that co-adsorption of co-adsorbents with dye

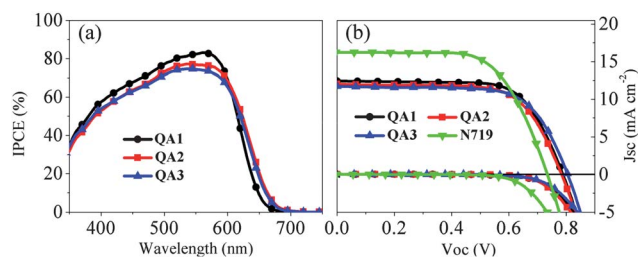


Fig. 2 (a) IPCE spectra for DSSCs based on dyes **QA1–3**. (b) I – V curves for DSSCs based on dyes **QA1–3** and **N719** under light (100 mW cm⁻² simulated AM 1.5 solar light) and dark.

Table 2 Photovoltaic performance of untreated DSSCs based on **QA1**, **QA2**, **QA3** and **N719** and CDCA with different concentrations of 10 mM, 20 mM and 30 mM co-adsorbed DSSCs based on **QA1**^a

Dye	Concentration of CDCA/mM ⁻¹	J_{sc} /mA ⁻¹ cm ⁻²	V_{oc} /mV ⁻¹	FF	η (%)
QA1 ^b	0	12.42	776	0.71	6.80
QA2 ^b	0	12.06	773	0.69	6.39
QA3 ^b	0	11.78	794	0.69	6.46
QA1 ^b	10	12.82	792	0.73	7.41
QA1 ^b	20	13.25	804	0.73	7.70
QA1 ^b	30	12.30	813	0.72	7.23
N719 ^c	0	16.33	726	0.66	7.86

^a Measured under irradiation of AM 1.5 simulated solar light (100 mW cm⁻²) at room temperature, 14 μ m film thickness, 0.28 cm² working area, electrolyte containing: 0.1 M LiI + 0.05 M I_2 + 0.6 M DMPII + 0.5 M TBP in acetonitrile. ^b The concentration of **QA** dyes is 3×10^{-4} M in THF. ^c The concentration of **N719** is 3×10^{-4} M in ethanol.

molecules which suffer from aggregation can improve solar cell performance significantly.¹⁰ Since **QA1** exhibits the best performance among the three dyes studied in this work, we focus on the optimization of **QA1**-based DSSCs using a co-adsorption strategy, and the data are summarized in Table 2 (the I - V curves are shown in Fig. S3†). As shown in Fig. S3†, the short-circuit photocurrent (J_{sc}) of **QA1**-based DSSC increases from 12.42 to 13.25 mA cm⁻² with 10 and 20 mM CDCA, respectively, and then slightly decreases with further increasing CDCA to 30 mM. One explanation is that the amount of adsorbed dye on the TiO₂ surface is reduced by the co-adsorbents of CDCA (as shown in Fig. S4†), resulting in a loss in light harvesting and thus a decreased short-circuit photocurrent. The open-circuit voltage in the DSSCs with **QA1** is improved, indicating that the charge recombination process is effectively prohibited in the presence of CDCA. Resulting from the co-grafting of the two molecules, the formation of a mixed mono-layer should be more tightly packed than when the sensitizer is absorbed alone, providing an insulating barrier against back electron transfer more effectively from the TiO₂ conduction band to the electrolyte.^{43,44} As shown in Table 2, the highest power conversion efficiency could be obtained at 20 mM CDCA, in which **QA1** achieved an overall conversion efficiency of 7.70% ($J_{sc} = 13.25$ mA cm⁻², $V_{oc} = 804$ mV, FF = 0.73).

Electrochemical impedance spectroscopy

Electrochemical impedance spectroscopy (EIS) analysis is considered as a powerful tool to elucidate the electronic and ionic transport processes in DSSCs. Fig. 3 shows the EIS for DSSCs based on dyes **QA1–3** and 20 mM CDCA co-adsorbed DSSCs based on dye **QA1** under a forward bias of -0.70 V from 0.1 Hz to 100 KHz in the dark. As shown in Fig. 3a, the Nyquist diagram shows two semicircles in the measured frequency range, in which the larger semicircle located in the low-frequency region is assigned to the dark reaction impedance caused by charge transportation at the TiO₂-dye-electrolyte interface, and the other smaller semicircle located in the high-frequency region is attributed to the charge-transfer at the counter electrode.^{45,46} The radius of the larger semicircle increases in the order **QA2** < **QA1** < **QA3**, indicating that the electron recombination resistance increases from **QA2**, **QA1**, **QA3**. This result is in agreement with the observed shift in the V_{oc} value under standard global AM 1.5 illumination and in the dark. With an optimized dye **QA1** to be co-adsorbed with 20 mM CDCA, the **QA1**-based DSSCs show a

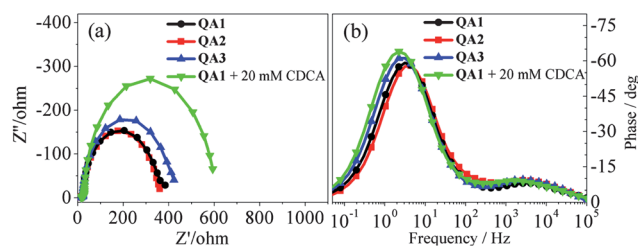


Fig. 3 Impedance spectra of untreated DSSCs based on dyes **QA1–3** and 20 mM CDCA co-adsorbed DSSCs based on dye **QA1** measured at -0.70 V bias in the dark. (a) Nyquist plots; (b) Bode phase plots.

larger semicircle after co-sensitization, which is reflected in the improvement shown in the V_{oc} .

Fig. 3b shows the Bode plots of the DSSCs based on **QA1–3**. All EIS Bode plots exhibit two peak features for the frequency investigated. The one at higher frequency corresponds to charge transfer at the Pt/electrolyte interface and meanwhile the other one at lower frequency corresponds to the charge transfer at the TiO₂/dye/electrolyte interface, which is related to the charge recombination rate and whose reciprocal is associated with the electron lifetime.⁴⁷ In Fig. 3b, the low frequency peak of **QA3** shows a lower frequency than those of **QA1** and **QA2**, indicating that **QA3**-based DSSCs have longer electron lifetimes, which leads to a lower rate of charge recombination. The electron lifetime values of **QA1–3** are 54.9 ms, 43.0 ms and 66.3 ms, respectively, likewise supporting the observed shift in the

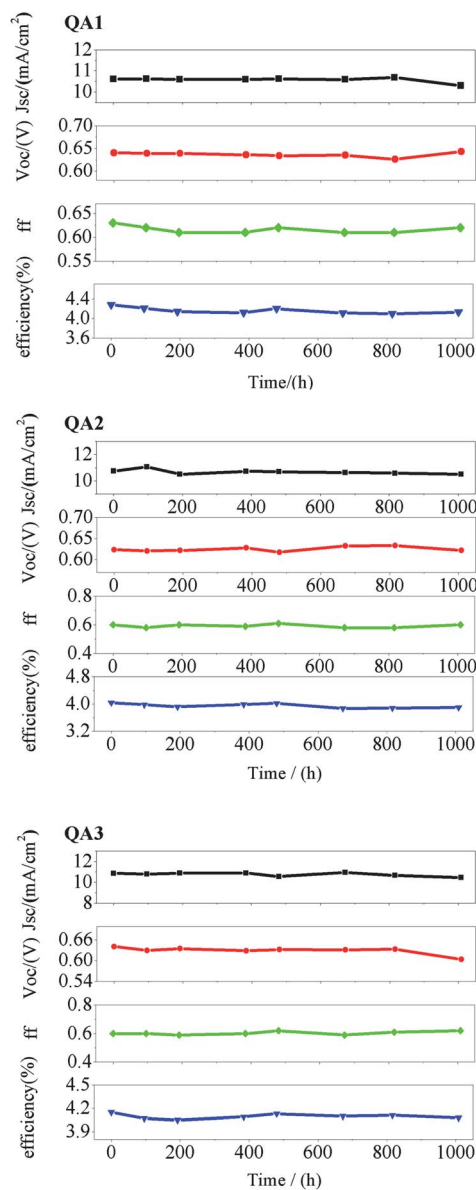


Fig. 4 Variations of photovoltaic parameters (J_{sc} , V_{oc} , FF, and η) with aging time for the DSSC device based on **QA1–3** with ionic-liquid electrolyte under visible-light soaking.

V_{oc} value under standard global AM 1.5 illumination and in the dark. Due to the slight blocking effect of the methoxy group, **QA3** based DSSCs show a higher V_{oc} than **QA1** and **QA2** based DSSCs, as a result of the enhanced electron lifetime. After co-sensitization with CDCA, the low frequency peak of **QA1** shows a lower frequency than before, and this indicates that the 20 mM CDCA co-sensitized **QA1**-based cell has a longer electron lifetime (79.6 ms), which leads to a lower rate of charge recombination and thus an improved V_{oc} .

Long-term stability measurements of ionic liquid electrolyte based DSSCs

Long-term stability is considered as an important parameter for sustained cell operation for applications in the future. Hence, due to low volatility and high thermal stability, ionic-liquid based electrolytes are a better choice.⁴⁸ The DSSCs were prepared using 0.1 M iodine, 0.1 M lithium iodide, 0.45 M benzimidazole in 1-propyl-3-methyl imidazolium iodide as the redox electrolyte. The photovoltaic performances of **QA1–3** sensitized TiO₂ film electrodes with a solvent-free ionic liquid electrolyte under standard global AM 1.5 solar light conditions (100 mW cm⁻²) are shown in Fig. S5† and summarized in Table S5†. In accordance with DSSCs based on liquid electrolytes, the photovoltaic parameters of the **QA1** based DSSCs with ionic-liquid electrolytes show best performance of 4.28% ($J_{sc} = 10.60$ mA cm⁻², $V_{oc} = 640$ mV, FF = 0.63). The J_{sc} , V_{oc} and FF show little change over 1000 h in Fig. 4. Moreover, Fig. 4 reveals that the DSSCs based on **QA1–3** with an ionic-liquid electrolyte remained at 96%, 97%, 98% of the initial overall efficiency value after 1000 h of visible-light soaking, respectively, which could demonstrate the good stability of DSSCs based on quinacridone sensitizers.

Conclusion

In conclusion, three new metal-free quinacridone-based organic dyes with a furan unit (**QA1–3**) were conveniently prepared and characterized. It was found that the introduction of the triphenylamine group as the electron-donor brought about improved photovoltaic performance compared with methoxytriphenylamine and *N,N*-diphenyl-4-vinylbenzenamine for quinacridone dyes. Co-adsorption of CDCA can break up the dye aggregates, leading to an increase of the photocurrent density, and suppressing charge recombination, leading to increasing electron lifetimes and thus photovoltage. A maximum solar energy to electricity conversion efficiency of 7.70% ($J_{sc} = 13.25$ mA cm⁻², $V_{oc} = 804$ mV, FF = 0.73) under simulated AM 1.5 solar light irradiation (100 mW cm⁻²) with a 20 mM CDCA co-adsorbed DSSC based on **QA1** was obtained. Most importantly, the long-term stability of the quinacridone DSSCs with ionic-liquid electrolytes under 1000 h light-soaking was demonstrated. The quinacridone moiety and the furan ring have excellent planarity from the DFT calculations. In addition, as an alternative to thiophene, the furan ring can be advantageously incorporated into dye-sensitizers as a π -spacer and can improve the cell efficiency and stability. Our findings demonstrate that quinacridone-based organic sensitizers with a furan moiety are promising for the further improvement of the conversion efficiency of DSSCs owing to the original and versatile molecular design.

Acknowledgements

This work was supported by NSFC/China (2116110444 and 21172073), National Basic Research 973 Program (2011CB808400), the Fundamental Research Funds for the Central Universities (WJ0913001), and Ph.D. Programs Foundation of Ministry of Education of China (20090074110004).

Notes and references

- B. O'Regan and M. Grätzel, *Nature*, 1991, **353**, 737.
- F. Gao, Y. Wang, J. Zhang, D. Shi, M. Wang, R. Humphry-Baker, P. Wang, S. M. Zakeeruddin and M. Grätzel, *Chem. Commun.*, 2008, 2635.
- (a) J. H. Yum, I. Jung, C. Baik, J. Ko, M. K. Nazeeruddin and M. Grätzel, *Energy Environ. Sci.*, 2009, **2**, 100; (b) L. Y. Han, A. Islam, H. Chen, C. Malapaka, B. Chiranjeevi, S. Zhang, X. Yang and M. Yanagida, *Energy Environ. Sci.*, 2012, **5**, 6057.
- A. Mishra, M. K. Fischer and P. Bauerle, *Angew. Chem., Int. Ed.*, 2009, **48**, 2474.
- H. N. Tian, X. C. Yang, J. Y. Cong, R. K. Chen, J. Liu, Y. Hao, A. Hagfeldt and L. C. Sun, *Chem. Commun.*, 2009, 6288.
- H. N. Tian, X. C. Yang, R. K. Chen, A. Hagfeldt and L. C. Sun, *Energy Environ. Sci.*, 2009, **2**, 674.
- H. N. Tian, X. C. Yang, R. K. Chen, Y. Z. Pan, L. Li, A. Hagfeldt and L. C. Sun, *Chem. Commun.*, 2007, 3741.
- W. J. Wu, J. B. Yang, J. L. Hua, J. Tang, L. Zhang, Y. T. Long and H. Tian, *J. Mater. Chem.*, 2010, **20**, 1772.
- D. R. Cao, J. A. Peng, Y. P. Hong, X. M. Fang, L. Y. Wang and H. Meier, *Org. Lett.*, 2011, **13**, 1610.
- S. Y. Qu, W. J. Wu, J. L. Hua, C. Kong, Y. T. Long and H. Tian, *J. Phys. Chem. C*, 2010, **114**, 1343.
- F. L. Guo, S. Y. Qu, W. J. Wu, J. Li, W. J. Ying and J. L. Hua, *Synth. Met.*, 2010, **160**, 1767.
- T. Horieuchi, H. Miura, K. Sumioka and S. Uchida, *J. Am. Chem. Soc.*, 2004, **126**, 12218.
- W. H. Zhu, Y. Z. Wu, S. T. Wang, W. Q. Li, J. Chen, Z. S. Wang and H. Tian, *Adv. Funct. Mater.*, 2011, **21**, 756.
- W. Q. Li, Y. Z. Wu, X. Li, Y. S. Xie and W. H. Zhu, *Energy Environ. Sci.*, 2011, **4**, 1830.
- W. Q. Li, Y. Z. Wu, Q. Zhang, H. Tian and W. H. Zhu, *ACS Appl. Mater. Interfaces*, 2012, **4**, 1822.
- A. Yella, H. W. Lee, H. N. Tsao, C. Y. Yi, A. K. Chandiran, M. K. Nazeeruddin, E. W. G. Diau, C. Y. Yeh, S. M. Zakeeruddin and M. Grätzel, *Science*, 2011, **334**, 629.
- S. S. Labana and L. L. Labana, *Chem. Rev.*, 1967, **67**, 1.
- T. Beyerlein, B. Tiede, S. Forero-Lenger and W. Brütting, *Synth. Met.*, 2002, **130**, 115.
- A. R. Rabindranath, Y. Zhu, I. Heim and B. Tiede, *Macromolecules*, 2006, **39**, 8250.
- N. Koumura, Z. S. Wang, M. Miyashita, Y. Uemura, H. Sekiguchi, Y. Cui, A. Mori, S. Mori and K. Hara, *J. Mater. Chem.*, 2009, **19**, 4829.
- J. X. He, T. L. Chen, B. S. Kim, D. A. Poulsen, J. L. Mynar, J. M. Frechet and B. Ma, *ACS Appl. Mater. Interfaces*, 2010, **2**, 2679.
- Z. J. Ning and H. Tian, *Chem. Commun.*, 2009, 5483.
- J. X. He, W. J. Wu, J. L. Hua, Y. H. Jiang, S. Y. Qu, J. Li, Y. T. Long and H. Tian, *J. Mater. Chem.*, 2011, **21**, 6054.
- Z. J. Ning, Y. Fu and H. Tian, *Energy Environ. Sci.*, 2010, **3**, 1170.
- J. Tang, J. L. Hua, W. J. Wu, J. Li, Z. G. Jin, Y. T. Long and H. Tian, *Energy Environ. Sci.*, 2010, **3**, 1736.
- R. Katoh, A. Furube, S. Mori, M. Miyashita, K. Sunahara, N. Koumura and K. Hara, *Energy Environ. Sci.*, 2009, **2**, 542.
- U. F. Bunz, *Angew. Chem., Int. Ed.*, 2010, **49**, 5037.
- B. Walker, A. B. Tamayo, X. D. Dang, P. Zalar, J. H. Seo, A. Garcia, M. Tantiwiwat and T. Q. Nguyen, *Adv. Funct. Mater.*, 2009, **19**, 3063.
- T. Yamamoto, Z.-H. Zhou, T. Kanbara, M. Shimura, K. Kizu, T. Maruyama, Y. Nakamura, T. Fukuda, B.-L. Lee, N. Ooba, S. Tomaru, T. Kurihara, T. Kaino, K. Kubota and S. Sasaki, *J. Am. Chem. Soc.*, 1996, **118**, 10389.
- Y. Araki, T. Wada, O. Yoshikawa, T. Sagawa, S. Yoshikawa and H. Imahor, *J. Phys. Chem. C*, 2009, **113**, 10798.

- 31 J. T. Lin, P.-C. Chen, Y.-S. Yen, Y.-C. Hsu, H.-H. Chou and M.-C. P. Yeh, *Org. Lett.*, 2009, **11**, 97.
- 32 R. Li, X. J. Lv, D. Shi, D. F. Zhou, Y. M. Cheng, G. L. Zhang and P. Wang, *J. Phys. Chem. C*, 2009, **113**, 7469.
- 33 J. Y. Mao, F. L. Guo, W. J. Ying, W. J. Wu, J. Li and J. L. Hua, *Chem.-Asian J.*, 2012, **7**, 982.
- 34 (a) S. Y. Qu and H. Tian, *Chem. Commun.*, 2012, **48**, 3039; (b) S. Y. Qu, B. Wang, F. L. Guo, J. Li, W. J. Wu, C. Kong, Y. T. Long and J. L. Hua, *Dyes Pigm.*, 2012, **92**, 1384; (c) S. Y. Qu, J. L. Hua and H. Tian, *Sci. China: Chem.*, 2012, **55**, 677.
- 35 C. H. Woo, P. M. Beaujuge, T. W. Holcombe, O. P. Lee and J. J. Frechet, *J. Am. Chem. Soc.*, 2010, **132**, 15547.
- 36 C. Sakong, S. H. Kim, S. B. Yuk, J. Y. Kim, S. W. Park, M. J. Ko and J. P. Kim, *Bull. Korean Chem. Soc.*, 2011, **32**, 2553.
- 37 H. Im, S. Kim, C. Park, S. Jang, C. Kim, K. Kim, N. Park and C. Kim, *Chem. Commun.*, 2010, **46**, 1335.
- 38 M. Nazeeruddin, A. Kay, I. Rodicio, R. Humphry-Baker and M. Grätzel, *J. Am. Chem. Soc.*, 1993, **115**, 6382.
- 39 T. Horiuchi, H. Miura and S. Uchida, *Chem. Commun.*, 2003, 3036.
- 40 M. Guo, P. Diao, Y. J. Ren, F. Meng, H. Tian and S. M. Cai, *Sol. Energy Mater. Sol. Cells*, 2005, **88**, 23.
- 41 Z. S. Wang, N. Koumura, Y. Cui, M. Takahashi, H. Sekiguchi, A. Mori, T. Kubo, A. Furube and K. Hara, *Chem. Mater.*, 2008, **20**, 3993.
- 42 K. M. Karlsson, X. Jiang, S. K. Eriksson, E. Gabrielsson, H. Rensmo, A. Hagfeldt and L. C. Sun, *Chem.-Eur. J.*, 2011, **17**, 6415.
- 43 Z. S. Wang, Y. Cui, Y. Dan-oh, C. Kasada, A. Shinpo and K. Hara, *J. Phys. Chem. C*, 2007, **111**, 7224.
- 44 J. He, G. Benko, F. Korodi, T. Polivka, R. Lomoth, B. Akermark, L. C. Sun, A. Hagfeldt and V. Sundström, *J. Am. Chem. Soc.*, 2002, **124**, 4922.
- 45 L. Y. Han, N. Koide, Y. Chiba, A. Islam, R. Komiya, N. Fuke, A. Fukui and R. Yamanaka, *Appl. Phys. Lett.*, 2005, **86**, 213501.
- 46 Q. Wang, J. Moser and M. Grätzel, *J. Phys. Chem. B*, 2005, **109**, 14945.
- 47 L. Y. Lin, C. H. Tsai, K. T. Wong, T. W. Huang, L. Hsieh, S. H. Liu, H. W. Lin, C. C. Wu, S. H. Chou, S. H. Chen and A. I. Tsai, *J. Org. Chem.*, 2010, **75**, 4778.
- 48 H. Qin, S. Wenger, M. F. Xu, F. F. Gao, X. Y. Jing, P. Wang, S. M. Zakeeruddin and M. Grätzel, *J. Am. Chem. Soc.*, 2008, **130**, 9202.